Microscopic theory of longitudinal sound velocity in charge ordered manganites

2009 J. Phys.: Condens. Matter 21 416001

(http://iopscience.iop.org/0953-8984/21/41/416001)

J. Phys.: Condens. Matter **21** (2009) 416001 (9pp) doi:10.1088/0953-8984/21/41/416001

Microscopic theory of longitudinal sound velocity in charge ordered manganites

G C Rout[1,3] **and S Panda**[2]

[1] Condensed Matter Physics Group, PG Department of Applied Physics and Ballistics, FM University, Balasore 756 019, India
[2] Trident Academy of Technology, F2/A, Chandaka Industrial Estate, Bhubaneswar 751 024, India

E-mail: gcr@iopb.res.in

Received 30 April 2009, in final form 1 September 2009
Published 23 September 2009
Online at stacks.iop.org/JPhysCM/21/416001

Abstract

A microscopic theory of longitudinal sound velocity in a manganite system is reported here. The manganite system is described by a model Hamiltonian consisting of charge density wave (CDW) interaction in the e_g band, an exchange interaction between spins of the itinerant e_g band electrons and the core t_{2g} electrons, and the Heisenberg interaction of the core level spins. The magnetization and the CDW order parameters are considered within mean-field approximations. The phonon Green's function was calculated by Zubarev's technique and hence the longitudinal velocity of sound was finally calculated for the manganite system. The results show that the elastic spring involved in the velocity of sound exhibits strong stiffening in the CDW phase with a decrease in temperature as observed in experiments.

(Some figures in this article are in colour only in the electronic version)

1. Introduction

Ever since the discovery of the colossal magnetoresistance (CMR) effect in hole doped manganites $R_{1-x}A_xMnO_3$ (R = trivalent rare earth; A = divalent alkaline-earth element), a considerable amount of research has been devoted to the investigation of microscopic mechanism of the CMR effect in this class of materials [1–4]. The system shows a negative CMR effect near the Curie temperature for low doping levels ($0.15 \leqslant x \leqslant 0.5$); but at higher doping ($0.5 \leqslant x \leqslant 0.85$) a charge ordering (CO) transition has been observed for several systems such as $R_{0.5}Sr_{0.5}MnO_3$ (R = La, Pr, Nd) [5–7], $Pr_{1-x}Ca_xMnO_3$ [8, 9], $La_{0.5}Sr_{1.5}MnO_4$ [10, 11] and $La_{1-x}Ca_xMnO_3$ ($0.5 < x < 0.8$) [12, 13]. The doped carriers are ordered below the charge ordering temperature (T_{CO}) which is usually associated with orbital ordering and antiferromagnetism (AFM). The system $La_{0.5}Ca_{0.5}MnO_3$ shows an unpredicted co-existence of ferromagnetism and incommensurate charge ordering with AFM transition temperature $T_C \approx 240$ K [14, 15]. With the anomalous magnetic transition occurring near T_{CO}, the lattice parameters show significant changes and the charge and orbit become ordered with a wavevector $q = 2\pi/a[1/2 - \epsilon, 0, 0]$ just below T_{CO} [16]. These features indicate that the competition between charge, spin, orbit and lattice degrees of freedom plays an important role in the electric, magnetic and structural properties in the charge ordering materials.

The recent experiments indicate charge disproportion (<1) [17, 18], exclude charge delocalization [19] and show that the charge modulation remains uniform when passing from commensurate to incommensurate doping [20]. A collective sliding of the charge system is observed at $x = 0.5$ [21]. All these results indicate that, in several manganites, the CO phase can be described [22] in terms of the charge density wave (CDW) model [23, 24]. The spectroscopic measurements on $Pr_{0.7}Ca_{0.3}MnO_3$ [25] show a peak at 25 cm^{-1} and a broad shoulder at lower frequencies which attribute collective excitations to the CDW. In the optical conductivity of four different manganites with commensurate charge, a strong CDW excitation peak appears in the meV range below T_{CO} for frequency $\omega > 2\Delta_C$, with a CDW gap of $2\Delta_C$ ($T = 0$) $\simeq$ 800 cm^{-1} or 0.1 meV for LCMO and ~0.2 meV in $Nd_{1/2}Ca_{1/2}MnO_3$ (NCMO) [26]. Further, the calculated Fermi surface [27] shows pronounced nesting features along the Γ–X direction in the undoped case, and this implies a possible charge or spin density wave instability in the half-metallic double layered compound $La_{1-2x}Sr_{2-2x}Mn_2O_7$ [27].

[3] Author to whom any correspondence should be addressed.

It is well known that ultrasonic measurement is a very sensitive probe for all kinds of phase transitions, including ferroelectric, magnetic and structural ones. It has also been proved to be successful in studying the electron–phonon coupling systems and spin–phonon coupling in hole doped magnetoresistive manganites [13, 28]. Ultrasonic sound velocity and attenuation on the system $La_{1-x}Ca_xMnO_3$ [29] shows a dramatic stiffening below T_{CO}. It has been suggested that this structural transition is due to the Jahn–Teller distortion of oxygen octahedra around the Mn-ion and is related to the charge ordering transition. Recently Zainullina *et al* [30] have reported the longitudinal sound measurements on $La_{0.80}A_{0.20}MnO_3$ showing a Curie temperature $T_C \simeq 300$ K and structural transition at $T_S = 95$ K for A = Sr and $T_S = 190$ K for A = Ba. More recently Ewe *et al* [31] have observed a metal–insulator transition at $T_{IM} \approx 272$ K in the measurement of longitudinal sound velocity in $La_{0.67}Ca_{0.33}MnO_3$. The magnetic ordering effect in the phonon spectra of $RMnO_3$ compounds was investigated recently [32] by a model study based on spin–phonon interaction.

In view of the large number of experimental data available on ultrasonic studies in manganites, it becomes important to carry out model studies of ultrasonic sound velocity, ultrasonic attenuation and Raman spectra to interpret the experimental results. Recently Rout *et al* have reported a model study on manganites and discussed the effect of the Jahn–Teller interaction on the conductance current and magnetic response in CMR systems [33, 34]. In the present paper, we propose a model study which includes the CDW state in the itinerant e_g band and the exchange interaction between the spins of e_g and the core level t_{2g} spin along with the Heisenberg interaction among the spins of the core t_{2g} states. We calculate the phonon Green's function and hence the velocity of sound for the manganite system. The rest of the work is organized as follows. The model Hamiltonian is discussed in section 2. The phonon Green's function is calculated in section 3. The longitudinal velocity of sound for the system is calculated in section 4 in the long wavelength limit. The results and discussion are presented in section 5 and finally the conclusion in section 6.

2. Theoretical model

In the octahedral environment of the Mn ion in the manganites, the d levels of the Mn ions split into low lying three-fold degenerate t_{2g} states and higher energy two-fold degenerate e_g states separated by the crystal field energy (∼2 eV). In $LaMnO_3$, the four 3d electrons of Mn^{3+} are in a high spin ($S = 2$) state and the inter-orbital Coulomb energy is large. The three t_{2g} electrons can have a total spin $S = 3/2$ and are effectively ferromagnetically coupled with the e_g electron spin via the Hund rule coupling J, which is estimated to be large (∼2–3 eV). On doping with a divalent alkaline-earth metal which substitutes for the trivalent rare earths, a fraction x of sites has Mn^{4+} ions. Every site Mn^{3+} (with four 3d electrons) has the occupation probability of $(1 - x)$. Thus, the three t_{2g} electrons exhibit low spin behaviour. The low energy behaviour is determined by the e_g electrons. The Hamiltonian of the e_g band electron representing the hopping term is given by

$$H_c = \sum_{k,\sigma} (\epsilon(k) - \mu - B\sigma) c^\dagger_{k,\sigma} c_{k,\sigma} \tag{1}$$

where $\epsilon(k) = -2t_0(\cos k_x + \cos k_y)$ is the band energy with $2t_0$ as the nearest neighbour hopping integral and μ is the chemical potential. Here B is the external magnetic field, with $\sigma = 1$ for spin up and $\sigma = -1$ for spin down. The operator $c^\dagger_{k\sigma}(c_{k\sigma})$ is the creation (annihilation) operator of the e_g electrons. Peierls-type periodic lattice distortion in the system is associated with a spatially periodic modulation of the electronic charge density, called the charge density wave (CDW). The wavevector Q of the CDW is related to the Fermi wavevector k_F by $Q = 2k_F$, and consequently the formation of a CDW state opens up a gap at the Fermi level, lowering the kinetic energy of the conduction electrons. The Hamiltonian representing the CDW in the e_g band is given by

$$H_{CDW} = \Delta_C \sum_{k,\sigma} c^\dagger_{k+Q,\sigma} c_{k,\sigma} \tag{2}$$

where Δ_C is the CDW order parameter. The CDW state has a superperiodicity such that Q becomes the new reciprocal lattice vector with a corresponding reduced Brillouin zone (BZ). This satisfies the nesting property $\epsilon_{k\pm Q} = -\epsilon_k$, with a periodic wavevector Q. As mentioned earlier, one strong interaction at each site j is effectively described as ferromagnetic Hund rule coupling between t_{2g} spins $\mathbf{S}^d_j$ and e_g spins $\boldsymbol{\sigma}^c_j$, namely

$$H^{ex}_{cd} = -J \sum_{j\sigma} \boldsymbol{\sigma}^c_j \cdot \mathbf{S}^d_{j\sigma} \tag{3}$$

where J is the ferromagnetic exchange interaction ($J > 0$). Within the mean-field approximation in the Ising limit, the Hamiltonian can be written in terms of the dynamic electron operators as

$$H^{ex}_{cd} = \frac{JM^d}{2} \sum_{k,\sigma} \sigma c^\dagger_{k,\sigma} c_{k,\sigma} + \frac{JM^c}{2} \sum_{k,\sigma} \sigma d^\dagger_{k,\sigma} d_{k,\sigma} \tag{4}$$

where M^d and M^c are the z-components of the magnetization of the core electrons and band electrons respectively. The Heisenberg type direct spin–spin interaction among the core t_{2g} electrons is given by

$$H_m = -J_H \sum_{ij\sigma} \mathbf{S}^d_{i\sigma} \cdot \mathbf{S}^d_{j\sigma}. \tag{5}$$

Within the Ising limit, the Hamiltonian H_m can be written in terms of the z-component of magnetization M^d for the core electrons and its dynamic electron operators as

$$H_m = \frac{J_H M^d}{2} \sum_{k,\sigma} \sigma d^\dagger_{k,\sigma} d_{k,\sigma}. \tag{6}$$

The Hamiltonian of the localized core t_{2g} band electrons is given by

$$H_d = \sum_{k,\sigma} (\epsilon_d - B\sigma)\, d^\dagger_{k,\sigma}\, d_{k,\sigma} \tag{7}$$

where ϵ_d is the position of the t_{2g} core level with respect to the Fermi level ($\epsilon_F = 0$) and $d^\dagger_{k,\sigma}(d_{k,\sigma})$ is the creation (annihilation) operator of the core electron. The Fourier-transformed Hamiltonian describing the phonon coupling of the itinerant e_g band electrons is written as

$$H_{\text{el-ph}} = \sum_{k,q,\sigma} f(q) c^\dagger_{k+q,\sigma} c_{k,\sigma} A_q \tag{8}$$

with $A_q = b_q(t) + b^\dagger_{-q}(t)$, where b_q ($b^\dagger_{-q}$) is the phonon annihilation (creation) operator. The electron–phonon coupling constant is given by $f(q) = |\bar{q}|/\sqrt{(2N_0 M\omega_q)\epsilon_q}$, where ϵ_q is the Fourier transform of $\partial t_{ij}/\partial\epsilon_i$. The free phonon Hamiltonian with phonon energy ω_q of phonon wavevector q is

$$H_{\text{ph}} = \sum_q \omega_q b^\dagger_q b_q \tag{9}$$

in the harmonic approximation. The total Hamiltonian is written as

$$H = H_c + H_{\text{CDW}} + H^{\text{ex}}_{cd} + H_m + H_d + H_{\text{el-ph}} + H_{\text{ph}}. \tag{10}$$

3. Calculation of the phonon Green's function

The double-time phonon Green's function $D_{q,q'}(t,t')$ is evaluated by Zubarev's technique [35] using the equation of motion method. The phonon Green's function is defined as

$$\begin{aligned} D_{q,q'}(t,t') &= \langle\langle A_q(t); A_{q'}(t')\rangle\rangle \\ &= -\mathrm{i}\Theta(t,t')\langle[A_q(t); A_{q'}(t')]\rangle. \end{aligned} \tag{11}$$

We construct the equations of motion of the Green's function $D_{q,q'}(t,t')$ as

$$\begin{aligned} -\frac{\mathrm{d}^2 D_{q,q'}(t,t')}{\mathrm{d}t^2} &= 2\omega_q\delta_{-q,q'}\delta(t-t') \\ &\quad + 2\omega_q \sum_{k\sigma} f(-q) D_{1,k-q,k}(t-t') + \omega_q^2 D_{q,q'}(t-t'). \end{aligned} \tag{12}$$

The Green's function containing the electron and phonon operators is defined as

$$D_{1,k-q,k}(t-t') = \langle\langle c^\dagger_{k-q,\sigma} c_{k,\sigma}; A_{q'}(t')\rangle\rangle. \tag{13}$$

The Fourier transform of Green's functions in equation (12) is given as

$$D_{q,q'}(\omega) = D^0_q(\omega)\delta_{-q,q'} + 2\pi D^0_q(\omega) \sum_{k,\sigma} f(-q) D_{1,k-q,k}(\omega) \tag{14}$$

where the free phonon propagator is $D^0_q(\omega) = (\omega_q/\pi)[\omega^2 - \omega_q^2]^{-1}$. Taking the equation of motion of Green's function in equation (13) and its Fourier transform we get

$$\begin{aligned} D_{1,k-q,k}(\omega) &= 2\pi D^0_{q'}(\omega) \\ &\quad \times \sum_{k',\sigma'} f(-q')\Gamma(k-q, k'-q', \sigma, \sigma', \omega). \end{aligned} \tag{15}$$

On substitution of equation (15) in (14), $D_{q,q'}(\omega)$ reduces to

$$D_{q,q'}(\omega) = D^0_q(\omega)\delta_{q,q'} + 4\pi^2 D^0_q(\omega)\chi_{q,q'}(\omega) D^0_{q'}(\omega). \tag{16}$$

Applying Dyson's approximation to equation (16), the phonon Green's function is evaluated in the closed form as

$$D_{q,q'}(\omega_q) = \frac{\omega_q}{\pi}\left[\omega^2 - \omega_q^2 - \sum(\omega, q)\right]^{-1} \tag{17}$$

where $\sum(\omega, q) = 4\pi\omega_q\chi_{q,q}(\omega)$ is the phonon self-energy and the electron response function $\chi_{q,q}(\omega)$ is written as

$$\chi_{q,q}(\omega) = f^2(-q)\sum_{k,\sigma}\Gamma(k,q,\omega) \tag{18}$$

with,

$$\Gamma(k,q,\omega) = \sum_{k',\sigma'}\Gamma(k,k',q,q',\omega). \tag{19}$$

For simplicity, we drop the functional parameters like k, k', q, q' and ω from the Green's function $\Gamma(k,k',q,q',\omega)$ and other higher order Green's functions Γ_i. Now it is seen that the Green's function Γ defined in equation (19) is a two-particle Green's function and is coupled to other three two-particle Green's functions such as $\Gamma_1, \Gamma_2, \Gamma_3$ which are defined in terms of the electron operators αs and β as

$$\begin{aligned} \Gamma &= \langle\langle\alpha^a, \beta\rangle\rangle_\omega; & \Gamma_1 &= \langle\langle\alpha^b, \beta\rangle\rangle_\omega \\ \Gamma_2 &= \langle\langle\alpha^c, \beta\rangle\rangle_\omega; & \Gamma_3 &= \langle\langle\alpha^d, \beta\rangle\rangle_\omega. \end{aligned} \tag{20}$$

These α and β-operators are written in abbreviated form as

$$\begin{aligned} \alpha^a &= c^\dagger_{k-q,\sigma} c_{k,\sigma}; & \alpha^b &= c^\dagger_{k-q-Q,\sigma} c_{k,\sigma} \\ \alpha^c &= c^\dagger_{k-q,\sigma} c_{k-Q,\sigma}; & \alpha^d &= c^\dagger_{k-q-Q,\sigma} c_{k-Q,\sigma} \\ & & \beta &= c_{k'-q,\sigma} c_{k',\sigma}. \end{aligned} \tag{21}$$

The coupled equations for the Green's functions Γ, Γ_1, Γ_2 and Γ_3 are evaluated as

$$\begin{aligned} (\omega + \epsilon_{k-q,\sigma} - \epsilon_{k,\sigma})\Gamma &= \frac{A^a}{2\pi} - \Delta_C\Gamma_1 + \Delta_C\Gamma_2 \\ (\omega + \epsilon_{k-q-Q,\sigma} - \epsilon_{k,\sigma})\Gamma_1 &= \frac{A^b}{2\pi} - \Delta_C\Gamma + \Delta_C\Gamma_3 \\ (\omega + \epsilon_{k-q,\sigma} - \epsilon_{k-Q,\sigma})\Gamma_2 &= \frac{A^c}{2\pi} - \Delta_C\Gamma_3 + \Delta_C\Gamma \\ (\omega + \epsilon_{k-q-Q,\sigma} - \epsilon_{k-Q,\sigma})\Gamma_3 &= \frac{A^d}{2\pi} - \Delta_C\Gamma_2 + \Delta_C\Gamma_1. \end{aligned} \tag{22}$$

The above coupled equations involve expressions like A^a, A^b, A^c and A^d, which are defined as

$$\begin{aligned} A^a &= \langle[\alpha^a, \beta]\rangle; & A^b &= \langle[\alpha^b, \beta]\rangle \\ A^c &= \langle[\alpha^c, \beta]\rangle; & A^d &= \langle[\alpha^d, \beta]\rangle. \end{aligned}$$

These thermal expectation values of the number operators are evaluated explicitly by using the commutation relations valid for fermions and are given below:

$$\begin{aligned} A^a &= \delta_{\sigma,\sigma'}\delta_{-q,q'}\delta_{k-q,k'}(n^c_{k-q,\sigma} - n^c_{k,\sigma}) \\ A^b &= \delta_{\sigma,\sigma'}\delta_{-q-Q,q'}\delta_{k-q-Q,k'}(n^c_{k-q-Q,\sigma} - n^c_{k,\sigma}) \\ A^c &= \delta_{\sigma,\sigma'}\delta_{-q+Q,q'}\delta_{k-q,k'}(n^c_{k-q,\sigma} - n^c_{k-Q,\sigma}) \\ A^d &= \delta_{\sigma,\sigma'}\delta_{-q,q'}\delta_{k-q-Q,k'}(n^c_{k-q-Q,\sigma} - n^c_{k-Q,\sigma}). \end{aligned} \tag{23}$$

The electron occupation number present in the Green's functions is defined in general as $n^c_{k-q-Q,\sigma} = \langle c^\dagger_{k-q-Q,\sigma} c_{k,\sigma}\rangle$. The coupled equations given in equation (22) are solved in a closed form for the two-particle Green's function Γ. Substituting the value of Γ in phonon Green's function $D_{q,q}(\omega_q)$ given in equation (17), we can write

$$D_{q,q}(\omega) = \frac{\omega_q}{\pi}\left[\omega^2 - \omega_q^2 - \sum(\omega, q)\right]^{-1} \tag{24}$$

where the phonon self-energy reduces to

$$\sum(\omega, q) = \omega_q^2 s \int_{+W/2}^{-W/2} \mathrm{d}\epsilon_k \sum_\sigma G(\omega, \sigma, q, T). \tag{25}$$

Here the dimensionless electron–phonon coupling constant $s = N(0) f^2(-q)/\omega_q$. The function inside the integral in equation (25) is written as

$$G(\omega, \sigma, q, T) = \frac{[G_1(F_1^a - F_1^b) + G_2 F_2 - G_3 F_3]}{|D(\omega)|}. \tag{26}$$

The term in the denominator of the equation (26) is given by

$$|D(\omega)| = \omega^4 - \omega^2(\epsilon_+^2 + \epsilon_-^2 + 4\Delta_C^2) + \epsilon_+^2\epsilon_-^2.$$

Here, G_i $(i = 1, 2, 3)$ are written as

$$\begin{aligned} G_1 &= (\omega^2 - \epsilon_+^2)(\omega - \epsilon_-) - 4\omega\Delta_C^2 - 2\Delta_C\epsilon_+(\omega - \epsilon_-) \\ G_2 &= (\omega^2 - \epsilon_+^2 + 2\omega\Delta_C)(\omega - \epsilon_-)\frac{\epsilon_{k-q}}{E_{k-q}} \\ G_3 &= (\omega^2 - \epsilon_+^2 - 2\omega\Delta_C)(\omega - \epsilon_-)\frac{\epsilon_k}{E_k} \end{aligned} \tag{27}$$

where $\epsilon_\pm = (\epsilon_{k-q} \pm \epsilon_k)$ and $E_{k-q} = \sqrt{\epsilon_{k-q}^2 + \Delta_C^2}$. The F_is $(i = 1, 2, 3)$ appearing in the numerator of equation (26) are expressed in terms of the Fermi functions as given below.

$$\begin{aligned} F_1^a &= f(\beta\omega_{1,k-q,\sigma}) + f(\beta\omega_{2,k-q,\sigma}) \\ F_1^b &= f(\beta\omega_{1,k,\sigma}) + f(\beta\omega_{2,k,\sigma}) \\ F_2 &= f(\beta\omega_{1,k-q,\sigma}) - f(\beta\omega_{2,k-q,\sigma}) \\ F_3 &= f(\beta\omega_{1,k,\sigma}) - f(\beta\omega_{2,k,\sigma}) \end{aligned} \tag{28}$$

where the quasi-particle energies for electron wavevector k, the phonon wavevector q and the nesting wavevector Q are written as

$$\begin{aligned} \omega_{1,k-q-Q,\sigma} &= \omega_{1,k-q,\sigma} \qquad \omega_{2,k-q-Q,\sigma} = \omega_{2,k-q,\sigma} \\ \omega_{1,k-q,\sigma} &= E_{k-q} - \mu - \sigma B + \tfrac{1}{2} J M^d \\ \omega_{2,k-q,\sigma} &= -E_{k-q} - \mu - \sigma B + \tfrac{1}{2} J M^d. \end{aligned} \tag{29}$$

4. Velocity of sound

The velocity of sound in the crystal system can be calculated by equating the denominator of the phonon Green's function given in equation (24) to zero:

$$\left[\omega^2 - \omega_0^2 - \mathrm{Re}\sum(\omega, q \to 0)\right] = 0. \tag{30}$$

In the long wavelength limit we can write $\omega = vq$ and $\omega_q = v_0 q$ with v and v_0 representing the renormalized and bare velocity of sound in the system. Hence, the velocity of sound can be written as

$$\left(\frac{v}{v_0}\right)^2 = \left(\frac{\omega}{\omega_0}\right)^2 = 1 + s \times \int_{-W/2}^{+W/2} \mathrm{d}\epsilon_k \left[\sum_\sigma \mathrm{Re}\, G(\omega + \mathrm{i}\eta, q \to 0, \sigma)\right] \tag{31}$$

where η is the spectral width given to the frequency. In the long wavelength limit $\mathrm{Re}\, G$ is calculated explicitly and then the relative velocity $\tilde{v} = (v/v_0)$ is written as

$$\tilde{v}^2 = 1 + s \int_{-W/2}^{+W/2} \mathrm{d}\epsilon_k \left[\sum_\sigma \frac{G_4\{f(\beta\omega_{1,k,\sigma}) - f(\beta\omega_{2,k,\sigma})\}}{|D_1(\omega)|}\right] \tag{32}$$

where G_4 and $|D_1(\omega)|$ are given by

$$G_4 = 4\epsilon_k \Delta_C(\omega^2 - 4E_k^2)$$

and

$$|D_1(\omega)| = E_k\{(\omega^2 - 4E_k^2)^2 + 4\eta^2\omega^2\}.$$

The denominator $|D_1(\omega)|$ of equation (32) suggests that the velocity of sound exhibits a discontinuity at the energy $\omega \to 2E_k = 2\sqrt{(\epsilon_k^2 + \Delta_C^2)}$. In other words we expect a jump in velocity of sound at a CDW transition temperature corresponding to the CDW gap at $2\Delta_C$. It is to be noted here that the ferromagnetic transition in the Ising limit does not appear along with the CDW gap in the $|D_1(\omega)|$ appearing in the expression for velocity of sound given in equation (30). For the numerical results, all the energy parameters are normalized in terms of the conduction electron band width W. The dimensionless parameters are: the electron–phonon coupling 's', the exchange coupling $g = \frac{J}{W}$, the CDW coupling $g_1 = \frac{V_0 N(0)}{W}$, the Heisenberg coupling $g_2 = \frac{J_H}{W}$, the reduced temperature $t = \frac{k_B T}{W}$, the CDW parameter $e = \frac{\Delta_C}{W}$, the external magnetic field $b = \frac{B}{W}$, the reduced core level position $d = \frac{\epsilon_d}{W}$ and the reduced frequency $\Omega = \frac{\omega}{W}$.

5. Results and discussion

The clearest example of the influence of charge ordering (CO) of Mn^{3+} and Mn^{4+} is observed in the studies of $Pr_{0.5}Sr_{0.5}MnO_3$ [6]. This material has a ferromagnetic transition at $T_C = 270$ K. The charge ordering occurs with a simultaneous transition into an antiferromagnetic (AF) state at the CO/AF transition temperature at $T_{CO} = T_N = 140$ K and a large increase in resistivity due to the localization of charge carriers. Similar CO phenomena in other distorted perovskite manganese oxides have been reported in $La_{1-x}Ca_xMnO_3$ [36], $Pr_{1-x}Sr_xMnO_3$ [6, 37] and $Nd_{1-x}Sr_{1/2}MnO_3$ [7], for $x = 0.5$. In general, the cations of small ionic radii with (R, A) sites of $R_{1-x}A_xMnO_3$ cause a larger alternating tilting of MnO_6 octahedra and lead to a distortion dependent reduction of the one-electron band width. Consequently a small one-electron band width in the above cited manganites causes a

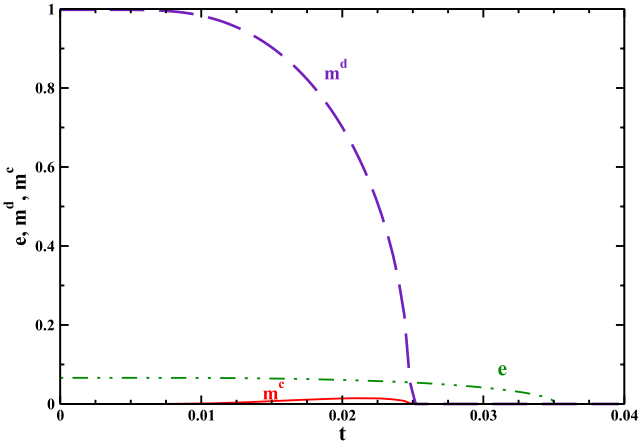

Figure 1. The temperature dependence of CDW gap (e), core-electron magnetization (m^d) and induced magnetization (m^c) in the e_g band for fixed CDW coupling $g_1 = 0.1035$, core–spin coupling $g_2 = 0.0995$ and c–d exchange coupling $g = 0.025$.

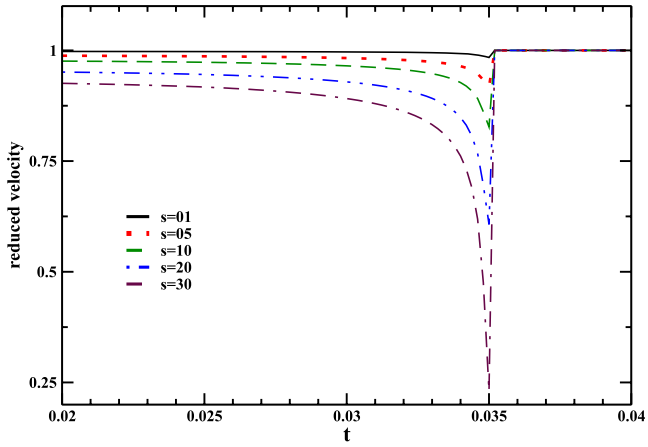

Figure 2. The curve of relative velocity ($\tilde{v}$) versus reduced temperature (t) for different values of electron–phonon coupling $s = 01, 05, 10, 20, 30$ for fixed values of Kondo coupling $g = 0.025$ and CDW coupling $g_1 = 0.1035$ in the absence of magnetic field ($b = 0$) at the zone centre.

charged state. The substitution of Ca on Pr in $PrMnO_3$ shows the influence of CO which persists, albeit in a distorted or locally clustered form, for $x = 0.30$ and 0.70 [38]. The magnetic and CO effects are decoupled for $x = 0.30$ in these compounds, for example the ordered AFM at $T_N = 170$ K developing at lower temperatures than the CO at $T_{CO} = 250$ K [39]. The electron doped manganites $R_{1-x}A_xMnO_3$ ($x > 0.5$) are in an AF or cluster glass (CG) state [40]. The important features of electron doped CMR manganites is their inhomogeneous electronic and magnetic states, sometimes revealed as a magnetic–electronic phase separation (PS) [40]. In the electron doped regime for $La_{0.16}Ca_{0.84}MnO_3$ there are inverted insulator–metal transitions. However, in this case the Néel and CO transition temperatures coincide. The end member of the electron doped system $CaMnO_3$ with $x = 1$ is a non-collinear antiferromagnetic insulator below $T_N \approx 125$ K. The nature of the negative magnetoresistance for electron doped manganites is still unclear. Our model study is applied below to study the longitudinal sound velocity for the magnetic and charge ordered mixed valence manganites as discussed earlier. For simplicity of calculation we have not considered the orbital ordering and AF interactions in our model study.

It is seen from the Fermi functions in equations (28) and quasi-particle energies in equations (29) that they involve the temperature dependent CDW gap Δ_C, mean-field magnetization m^d of core electrons and the induced e_g electron magnetization m^c. These three parameters are calculated from the electronic Hamiltonian in equation (10) in the absence of electron–phonon (EP) interaction and solved self-consistently and their interplay is reported in [32]. The temperature dependence of m^d, m^c and e is shown in figure 1. For the standard set of parameters $s = 10$, $g = 0.025$, $g_1 = 0.1035$, the ferromagnetic transition temperature appears at $t_c = 0.025$ ($T_C \sim 250$ K) and the CDW transition temperature at $t_d = 0.035$ ($T_{CO} \sim 350$ K). Under this condition, the transition temperature $t_d > t_c$ and there is an interplay of magnetization and CDW ordering below a temperature $t < t_c$. The system becomes paramagnetic for $t_c < t < t_d$ within the region in the presence of a CDW distortion and pure paramagnetic at $t > t_d$. The temperature dependence of (m^d) and the CDW gap (e) exhibit mean-field behaviour. It is observed that the strong core magnetization (m^d) induces a weak ferromagnetization m^c in the e_g band which is also modulated by the CDW interaction. As a result, the magnetization in m^c is suppressed considerably at lower temperatures due to the strong CDW gap [32]. This interplay is reflected here in the temperature dependent velocity of sound discussed below.

The temperature variation of relative velocity of sound of the manganite system exhibits anomalies at the CDW transition temperature (t_d) for certain physical parameters like phonon coupling to the conduction electrons (s), CDW coupling (g_1) and Kondo coupling (g). The velocity of sound is calculated at the BZ centre and at the zone boundary and the results are discussed below.

5.1. Velocity of sound at the zone centre at $q = 0$

Figure 2 shows the reduced velocity as a function of temperature for various EP coupling parameters $s = 1$–30. As phonon coupling s to the conduction band increases, the velocity of sound is suppressed throughout the temperature range up to the CDW transition temperature $t_d \sim 0.035$ ($T_{CO} \simeq 350$ K corresponding to the conduction band width of 1 eV). It is observed that for the EP parameter $s = 30$, the relative velocity becomes zero at $t = t_d$. This value of EP coupling is much higher in comparison to the case of $s = 0.11$–0.16 for CDW superconducting systems [41, 42] and $s = 0.0253$ for heavy-fermion systems in the normal phase [43–45]. Since Jahn–Teller (JT) coupling is significant for d^4 ions, such as Mn^{3+} in an octahedral oxygen environment, it seems natural to ascribe the huge lattice hardening in the CDW manganites to the larger electron–phonon coupling. Similar effects are observed in sound velocity measurement of $La_{0.33}Ca_{0.67}MnO_3$ [13]. The

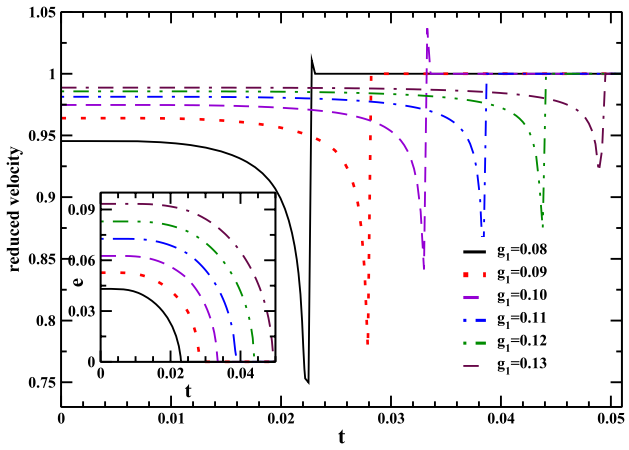

Figure 3. Plot of $\tilde{v}$ versus t for different values of CDW coupling $g_1 = 0.08, 0.09, 0.10, 0.11, 0.12, 0.13$ for fixed values of EP coupling $s = 10$ and Kondo coupling $g = 0.025$ at the zone centre. The inset shows the plot of the CDW parameter (e) versus t for the different values of g_1.

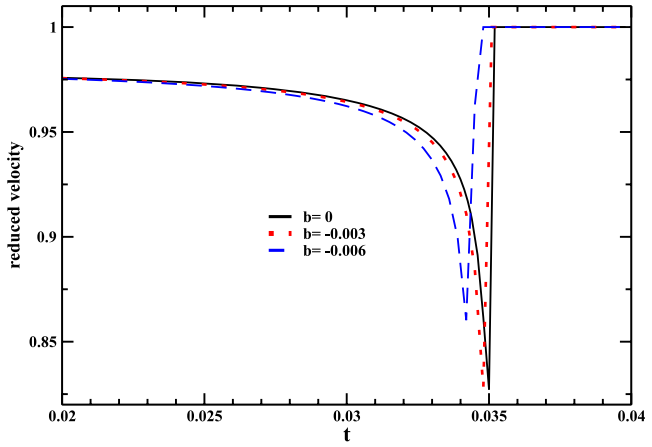

Figure 4. Plot of $\tilde{v}$ versus t for different values of external magnetic field $b = 0, -0.003$ and -0.006 at the zone centre.

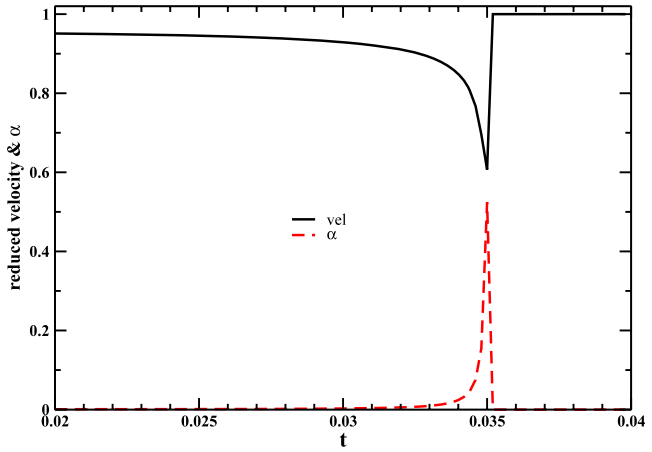

Figure 5. Plot of $\tilde{v}$ versus t and ultrasonic attenuation (α) versus t for constant EP coupling $s = 20$ at the zone centre.

suppression of frequency near t_d is very sharp, indicating the presence of a robust CDW transition. As the temperature increases from 0 K, the relative velocity remains nearly constant at low temperatures, falls sharply to a lower value at t_d and then suddenly jumps to the reduced value $\tilde{v} = 1$ for $t > t_d$ at higher temperatures above the CDW phase. For $t > t_d$, the frequency of the manganite system remains constant equal to the bare phonon frequency ω_0. The temperature dependence of longitudinal sound velocity from experiments on $La_{0.5}Ca_{0.5}MnO_3$ [13, 29] shows that there is slight softening on cooling down from a high temperature to the charge ordering temperature T_{CO}. However, nearly temperature independent behaviour of the sound velocity is observed in x-ray diffraction studies [46], as observed in our study. Just below T_{CO}, the sound velocity stiffens dramatically and recovers to a high value as temperature decreases from T_{CO}, as observed in longitudinal sound velocity and attenuation experiments [13, 29]. The dramatic softening and hardening in the lattice near the transition temperature indicates that the compound is intrinsically unstable like the CDW or Jahn–Teller type structural phase transition observed in electron diffraction experiment [12].

We know that the increase of CDW coupling g_1 enhances the CDW gap parameter e as well as its transition temperature t_d (see the inset of figure 3). This is reflected in the temperature dependence of relative velocity of the sound waves propagated in the manganite system as shown in figure 3. With the increase in the CDW coupling g_1 from 0.08 to 0.13, the magnitude of the velocity of sound increases towards its maximum value $\tilde{v} = 1$. Simultaneously the transition temperature is enhanced from $t_d \sim 0.022$ to $\sim$0.05 for the corresponding increase of g_1.

In figure 4, we show the sound velocity versus temperature for different external magnetic fields, $b = 0$ to (-0.006). We observe that the sound velocity is suppressed throughout the temperature range, the suppression being very large below the CDW transition (t_d). The CDW transition is also suppressed with the increase of magnetic field. The large anomaly appearing below t_d, which is very close to ferromagnetic transition, may lead to a magnetoresistivity anomaly in CMR manganites.

Figure 5 shows the temperature dependence of the reduced sound velocity ($\tilde{v}$) and ultrasonic attenuation (α) for longitudinal waves at a frequency $\Omega = 0.01$. Both the longitudinal sound velocity and ultrasonic attenuation show neither softening nor hardening on cooling down from a high temperature to the CDW transition temperature (t_d). Associated with a large decrease of sound velocity below t_d, there appears a pronounced increase in the attenuation near t_d. Just below the CDW temperature, the sound velocity stiffens dramatically and the attenuation decreases strikingly and levels off below a temperature $t \approx 0.031$. The dramatic stiffening of sound velocity and ultrasonic attenuation peak near t_d indicate that the compound is intrinsically unstable and the CDW phase transition takes place at t_d. Similar temperature dependence of change in longitudinal and transverse sound velocity as well as ultrasonic attenuation are observed for the manganite compound $La_{1-x}Ca_xMnO_3$ for $x = 0.50, 0.83$ at a frequency of 10 MHz near $T_{CO} \approx 180$ K [29].

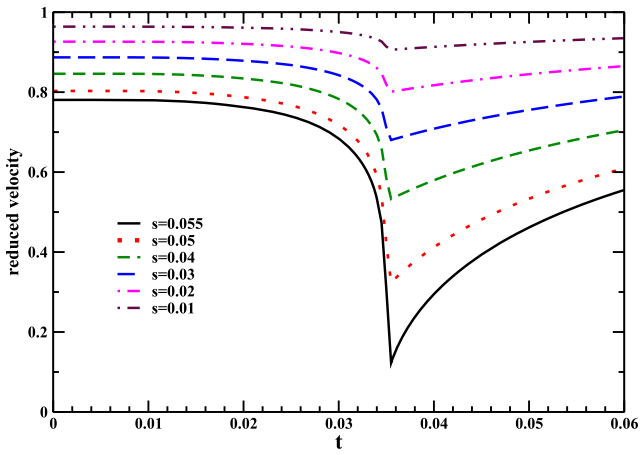

Figure 6. Plot of reduced velocity versus temperature for different values of EP coupling $s = 0.01, 0.02, 0.03, 0.04, 0.05$ and 0.055 at the zone boundary, other parameters remaining constant.

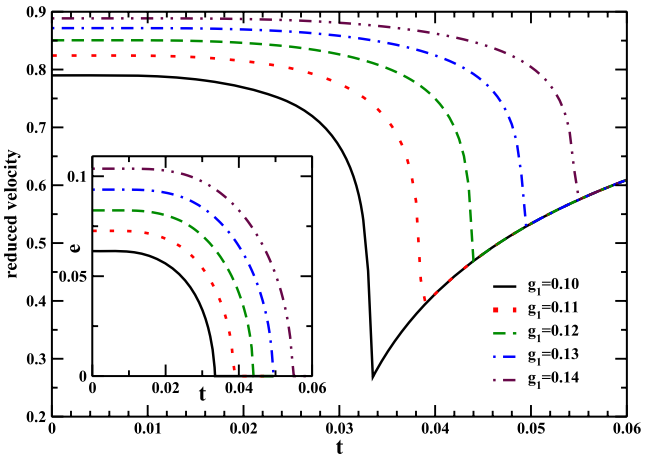

Figure 7. Plot of $\tilde{v}$ versus t for different values of $g_1 = 0.10, 0.11, 0.12, 0.13, 0.14$ for a fixed value of $s = 0.05$ at the zone boundary. The inset shows the plot of the CDW parameter (e) versus t for the different values of g_1.

5.2. Velocity of sound at the zone boundary at $q = Q$

In figure 6 we show the sound velocity versus temperature at the BZ boundary, i.e. at $q = Q$ for values of EP coupling $s = 0.01$–0.055. The sound velocity is suppressed throughout the temperature, both in the CDW phase $t < t_d$ and the paramagnetic phase at higher temperature (i.e. $t > t_d$). The higher EP coupling ($s \approx 0.058$) gives rise to a nearly zero magnitude of sound velocity at t_d. This shows that EP coupling for sound velocity at the BZ boundary is much smaller compared to its zone centre value. However, the value of EP coupling at the BZ boundary is comparable to $s = 0.11$–0.16 for CDW superconducting systems [41, 42] and to $s = 0.0235$ for heavy-fermion systems in the normal phase [43–45]. There is substantial stiffening as the CDW transition is approached from higher temperatures. There is also substantial stiffening of the sound velocity as the temperature is decreased from the CDW transition. This type of temperature dependence is observed for the system $La_{0.67}Sr_{0.33}MnO_3$ [13, 29]. Further, charge modulation at the wavevector $Q = (2\pi/a)[0.3, 0, 0]$ is also observed in this system from the electron diffraction measurements [13]. It is to be noted further that the sound velocity is suppressed more in the paramagnetic phase than in the low temperature CDW phase with increase in EP coupling. This indicates that the phonons couple strongly to the electrons in the paramagnetic phase than in the insulating CDW phase.

In figure 7 we show the temperature dependence of sound velocity for different CDW couplings $g_1 = 0.10$–0.14. With the increase of CDW coupling, the magnitude of sound velocity increases throughout the temperature range resulting in enhancement of the CDW transition temperature. The inset of the figure 7 shows the enhancement of the CDW gap as well as the CDW transition temperature with the increase of CDW coupling, and hence this enhancement is reflected in the corresponding enhancements in the sound velocity.

In figure 8, we show the effect of an external magnetic field on the temperature dependent velocity of sound at $q = Q$. In the paramagnetic phase (for $t > t_d$), the velocity of sound increases with application of a magnetic field, because the

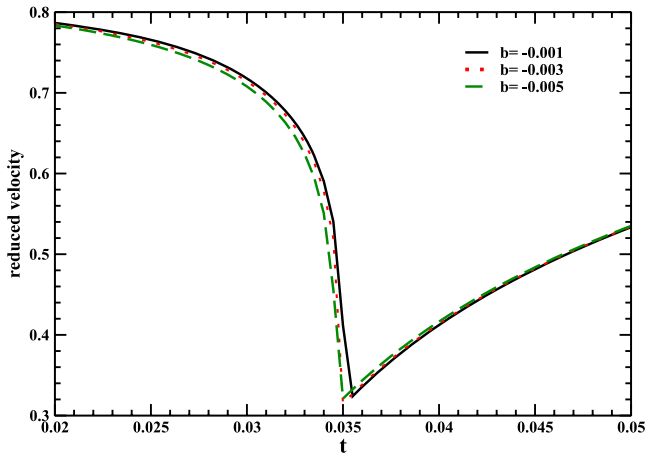

Figure 8. Plot of $\tilde{v}$ versus t for different values of external magnetic field $b = 0, -0.003$ and -0.005 at the zone boundary.

external field orders the electrons due to the Zeeman split and hence reduces the phonon coupling to the e_g electron resulting in the increase in sound velocity. But in the CDW phase (for $t < t_d$), the external magnetic field strongly interacts with the lattice and hence causes the suppression of the sound velocity with the application of the magnetic field. Recently Tomioka *et al* have reported that an applied field can cause a melting of charge ordering and then results in the insulator–metal (I–M) transition in the systems $Pr_{1-x}Ca_xMnO_3$ [47] as well as $Pr_{1/2}Sr_{1/2}MnO_3$ [6]. A field of a few tesla can also cause a lattice symmetry switching in related compounds $La_{1-x}Sr_xMnO_3$, $x = 0.17$ [48]. Such varieties of charge spin coupled properties in distorted perovskite manganese oxides can open the possibilities of controlling magnetic and transport properties and even lattice structure by an external magnetic field. Furthermore, the magnetostriction below and above T_C in mixed valent manganites is suppressed by thermal activation and the applied magnetic field [49].

Figure 9 shows the temperature dependence of the reduced sound velocity and ultrasonic attenuation for the BZ boundary

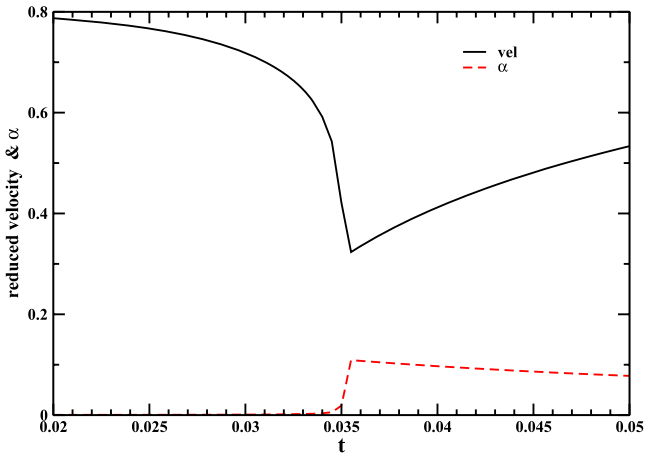

Figure 9. Plot of $\tilde{v}$ versus t and ultrasonic attenuation (α) versus t for constant EP coupling $s = 0.05$ at the zone boundary.

phonons at $q = Q$. The elastic spring involved in the sound velocity stiffens considerably below the CDW transition. With decrease in temperature from higher temperatures, attenuation slowly increases up to t_d in the paramagnetic phase, and just below the CDW transition temperature the attenuation decreases strikingly and levels off below $t = 0.033$. No attenuation peak is observed at t_d contrary to the observed attenuation peak for the $q = 0$ case.

6. Conclusion

We present a model study of the CDW interaction and its effect on some elastic properties of CMR manganites. The model Hamiltonian mainly consists of Heisenberg type direct spin–spin interactions among the core t_{2g} electrons and exchange interaction between spins of the itinerant e_g electrons and t_{2g} core electrons. The itinerant nature of the e_g electrons is controlled by a CDW insulating interaction present in the e_g band. We have explored possible consequences of the charge ordering phase for mixed valent manganites. From this model calculation, it is observed that CDW interaction completely suppresses the e_g electron magnetization (m^c) at low temperatures and interplays strongly with it near ferromagnetic transition. From the model Hamiltonian, we have calculated the temperature dependent longitudinal velocity of sound and ultrasonic attenuation at the BZ centre and at its boundary. In both cases the elastic spring involved in the velocity of sound exhibits strong stiffening on cooling down from the CDW transition temperature, as observed in experiments [13, 29, 46]. Associated with a dramatic change in sound velocity near CDW transition, the ultrasonic attenuation peak appears where the elastic spring involved in the sound velocity exhibits sharp stiffening. Further, it is also observed that strong EP coupling $s = 1$–20 exists in the zone centre results of sound velocity, while normal EP coupling ($s \approx 0.058$) exists for the zone boundary values of sound velocity. It is worthwhile comparing the results of this model with those of a stronger coupling model, for example the small polaron physics proposed by Millis *et al* [50]. Due to strong coupling of the electron to the local phonon modes, a small polaron is formed. At low temperatures the small polaron occupies a narrow band which narrows further as the temperature rises. Thus the band narrows on passing into high temperature state, while the criterion fails in the low temperature ferromagnetic state. This is reflected in the temperature dependent resistivity calculation based on the static Jahn–Teller effect [34]. Ibarra *et al* [49] have reported thermal expansion and magnetostriction results for a Y doped La–Ca–Mn–O compound which shows strong charge–lattice and spin–lattice coupling. They have observed charge localization (polaron effect) well above the Curie temperature $T_C \simeq 160$ K. This localization is gradual and produces a local distortion with decrease of temperature, as has been observed in other related compounds [6, 51]. Hence in the polaron model sound velocity would be renormalized well away from the transition, while the velocity of sound is strongly renormalized near the transitions in our charge ordered model. Thus this may be a method of distinguishing the two models.

References

[1] Tokura Y 2000 *Colossal Magnetoresistance Oxides* ed Y Tokura (New York: Gordon and Breach) chapter 1
[2] Salamon M B and Jaim M 2001 *Rev. Mod. Phys.* **73** 583
[3] Taraphder A 2007 *J. Phys.: Condens. Matter* **19** 125218
[4] Ramakrishnan T V 2007 *J. Phys.: Condens. Matter* **19** 125211
[5] Fujishiro H, Fukase T and Ikebe M 1998 *J. Phys. Soc. Japan* **67** 2582
[6] Tomioka Y, Asamitsu A, Moritomo Y, Kuwahara H and Tokura Y 1995 *Phys. Rev. Lett.* **74** 5108
[7] Kawano H, Kajimoto R, Yoshizawa H, Tomioka Y, Kuwahara H and Tokura Y 1997 *Phys. Rev. Lett.* **78** 4253
[8] Zimmermann M V, Hill J P, Gibbs D, Blume M, Casa D, Keimer B, Murakami Y, Tomioka Y and Tokura Y 1999 *Phys. Rev. Lett.* **83** 4872
[9] Tomioka Y, Asamitsu A, Kuwahara H and Moritomo Y 1996 *Phys. Rev.* B **53** R1689
[10] Murakami Y, Kawada H, Kawata H, Tanaka M, Arima T, Moritomo Y and Tokura Y 1998 *Phys. Rev. Lett.* **80** 1932
[11] Hess C, Buchner B, Hucker M, Gross R and Cheong S-W 1999 *Phys. Rev.* B **59** R10397
[12] Mori S, Chen C H and Cheong S-W 1998 *Nature* **392** 473
[13] Ramirez A P, Schiffer P, Cheong S-W, Chen C H, Bao W, Palstra T T M, Gammel P L, Bishop D J and Zegarski B 1996 *Phys. Rev. Lett.* **76** 3188
[14] Calvani P, Marzi G De, Dore P, Lupi S, Maselli P, D'Amore F, Gagliardi S and Cheong S-W 1998 *Phys. Rev. Lett.* **81** 4504
[15] Schiffer P, Ramirez A P, Bao W and Cheong S-W 1995 *Phys. Rev. Lett.* **75** 3336
[16] Radaelli P G, Cox D E, Marezio M and Cheong S-W 1997 *Phys. Rev.* B **55** 3015
[17] Subias G, Garcia J, Proietti M G and Blasco J 1997 *Phys. Rev.* B **56** 8183
[18] Garcia J, Sanchez M C, Subías G and Blasco J 2001 *J. Phys.: Condens. Matter* **13** 3229
[19] Martin J H, Garcia J, Subias G, Balsco J and Sanchez M C 2004 *Phys. Rev.* B **70** 024408
[20] Loudon J C, Cox S, Williams A J, Attfield J P, Littlewood P B, Midgley P A and Mathur N D 2005 *Phys. Rev. Lett.* **94** 097202
[21] Cox S, Singleton J, McDonald R D, Migliori A and Littlewood P B 2008 *Nat. Mater.* **7** 25
[22] Milward G C, Calderon M J and Littlewood P B 2005 *Nature* **433** 607

[23] Lee P A, Rice T M and Anderson P W 1974 *Solid State Commun.* **14** 703
[24] Grüner G 1988 *Rev. Mod. Phys.* **60** 1129
[25] Kida N and Tonouchi M 2002 *Phys. Rev.* B **66** 024401
[26] Nucara A, Maselli P, Calvani P, Sopracase R, Ortolani M, Gruener G, Guidi M C, Schade U and Garcia J 2008 *Phys. Rev. Lett.* **101** 066407
[27] Huang X Y, Mryasov O N, Novikov D L and Freeman A J 2000 *Phys. Rev.* B **62** 13318
[28] Zhu C, Zheng R, Su J and He J 1999 *Appl. Phys. Lett.* **74** 3504
[29] Zheng R K, Zhu C F, Xie J Q and Li X G 2000 *Phys. Rev.* B **63** 024427
[30] Zainullina R I, Bebenin N G, Mashkautsan V V, Ustinov V V and Mukovskii Ya M 2006 *J. Magn. Magn. Mater.* **300** e137
[31] Ewe L S, Hamadneh I, Salam H A and Abd-Shukor R 2008 *Physica* B **403** 2394
[32] Rout G C, Panda S and Behera S N 2009 *Physica* B at press
[33] Rout G C, Parhi N and Behera S N 2006 *Int. J. Mod. Phys.* B **20** 2093
[34] Rout G C, Parhi N and Behera S N 2007 *Physica* B **387** 259
[35] Zubarev D N 1960 *Sov. Phys.—Usp.* **3** 320
[36] Wollan E O and Koehler W C 1955 *Phys. Rev.* **100** 545
[37] Knizek K, Jirak Z, Pollen E, Zounova F and Vratislav S 1992 *J. Solid State Chem.* **100** 292
[38] Zirak Z, Vratislav S and Zajicek J 1979 *Phys. Status Solidi* **52** K39
[39] Lees M R, Barratt J, Balakrishnan G, Mck Paul D and Yethiraj M 1995 *Phys. Rev.* B **52** R14303
[40] Medvedeva I, Maignan A, Martin C, Bärner K, Raveau B, Bersenev Yu, Mushnikov N and Gerasimov E 2005 *Physica* B **365** 114
[41] Balseiro C A and Falicov L M 1980 *Phys. Rev. Lett.* **45** 662
[42] Rout G C, Pradhan B and Behera S N 2006 *Physica* C **444** 23
[43] Rout G C, Ojha M S and Behera S N 2005 *Physica* B **367** 101
[44] Rout G C, Ojha M S and Behera S N 2005 *Physica* B **370** 249
[45] Rout G C and Ojha M S 2007 *Physica* B **391** 299
[46] Radaelli P G, Cox D E, Marezio M, Cheong S-W, Schiffer P E and Ramirez A P 1995 *Phys. Rev. Lett.* **75** 4488
[47] Yoshizawa H, Kawano H, Tomioka Y and Tokura Y 1995 *Phys. Rev.* B **52** R13145
[48] Asamitsu A, Moritomo Y, Tomioka Y, Arima T and Tokura Y 1995 *Nature* **373** 407
[49] Ibarra M R, Algarabel P A, Marquina C, Blasco J and Garcia J 1995 *Phys. Rev. Lett.* **75** 3541
[50] Millis A J, Littlewood P B and Shraiman B I 1995 *Phys. Rev. Lett.* **74** 5144
[51] Moritomo Y, Tomioka Y, Asamitsu A, Tokura Y and Matsui Y 1995 *Phys. Rev.* B **51** 3297